

**Evidence for phonon-plasmon interaction in InN by Raman spectroscopy**

J. W. Pomeroy and M. Kuball

*H. H. Wills Physics Laboratory, University of Bristol, Bristol BS8 1TL, United Kingdom*

C. H. Swartz and T. H. Myers

*Department of Physics, West Virginia University, Morgantown, West Virginia 26505, USA*

H. Lu and W. J. Schaff

*Department of Electrical Engineering, Cornell University, Ithaca, New York 14853, USA*

(Received 6 March 2006; revised manuscript received 1 September 2006; published 8 January 2007)

The interaction between carriers and polar phonons in InN is investigated using Raman spectroscopy. An irreversible broadening and redshift of the  $595\text{ cm}^{-1}$   $A_1(\text{LO})$ -like phonon mode, observed after annealing the layer to 700 K, is direct evidence of phonon-plasmon interaction in InN. Variable field Hall effect measurements reveal that the InN layer is electrically heterogeneous and has at least three conduction layers exhibiting a reduction in mobility after annealing, consistent with the phonon-plasmon coupled mode broadening. A comparison between simulated and experimental coupled mode line shapes indicates that the mobility changes measured for bulk or interface carriers is not large enough to account for the experimentally observed annealing-induced broadening of the LO-like mode. We speculate that the observed  $A_1(\text{LO})$ -like mode broadening is related to surface conduction carriers.

DOI: [10.1103/PhysRevB.75.035205](https://doi.org/10.1103/PhysRevB.75.035205)

PACS number(s): 63.20.-e

**INTRODUCTION**

InN has attracted great interest for its possible applications in ultrafast electronic devices, solar cells, and optoelectronics.<sup>1</sup> However, it has only recently become possible to prepare high quality InN epilayers<sup>2</sup> and, as result, many material properties have only recently been reliably established, though many controversies still remain. The aspect investigated here is the nature of phonon-plasmon coupling in InN. Polar longitudinal optical (LO) phonons interact strongly with collective excitations of free carriers (plasmons) via their associated macroscopic electric fields. However, without exception, all Raman spectra reported for high-quality InN layers,<sup>3-9</sup> exhibit a phonon mode close to the predicted  $590\text{ cm}^{-1}$  LO phonon frequency.<sup>10</sup> Indeed, the mode observed close to the unscreened  $A_1(\text{LO})$  phonon frequency is always phononlike, despite the large range of carrier concentration and mobility typical for current material. As a result, in the past this mode has often been attributed to a *pure* (unscreened) phonon mode. Several authors have recently proposed that large wave vector scattering processes, likely due to impurity related scattering, may enable the InN longitudinal phonon-plasmon coupled mode (LPP) to approach the unscreened LO phonon frequency.<sup>4,7,8</sup> In this case, the InN LPP may be phononlike despite the high background free carrier concentration found in most InN films. A similar theory has been successfully applied to other semiconductor materials, for instance, GaAs (Ref. 11) and GaN.<sup>12</sup> However, there is as yet no direct evidence that the observed  $\sim 590\text{ cm}^{-1}$  mode is in fact a coupled mode and not a pure mode, e.g., originating from a surface depletion layer.<sup>4</sup> Other authors have suggested that an LPP has been observed close to the transverse optical (TO) phonon frequency in Raman scattering<sup>3</sup> and ellipsometry measurements.<sup>4</sup> Further investigation is therefore required.

To gain insight into the interaction between polar phonons and plasmons in InN, we report on Raman scattering in InN layers annealed between 80 K and 700 K. Annealing-induced changes in the LO-like phonon line shape are compared to carrier concentration and mobility changes determined by variable field Hall effect measurements. The Lindhard-Mermin dielectric function was used to calculate the LPP line shape for comparison to the experimental Raman spectra.

**EXPERIMENTAL METHOD**

The InN layers investigated here were deposited by molecular beam epitaxy (MBE) on a 300 nm GaN buffer, on a *c*-plane sapphire substrate, using the method described in Ref. 2. In the following, we concentrate on results obtained from a 500 nm thick InN layer. Raman spectra were recorded using a Renishaw inVia micro-Raman spectrometer and 785 nm laser diode excitation, probing a depth  $1/2\alpha$  of  $\sim 60\text{ nm}$ , where  $\alpha$  is the absorption coefficient reported in Ref. 13. To minimize laser heating of the sample, laser light was focused through a long working distance 50x objective into a  $2 \times 20\text{ }\mu\text{m}$  line; 15 mW of laser power was incident on the sample and no heating-induced phonon frequency shift was observed. Experiments were performed in the back-scattering geometry, allowing measurement of phonon modes with  $E_2$  and  $A_1(\text{LO})$  symmetry. The spectrometer spectral shift resolution and response width (FWHM) were  $\sim 0.1\text{ cm}^{-1}$  and  $2\text{ cm}^{-1}$ , respectively. The sample was placed in a Linkam TMS600 cryostat containing an  $N_2$  atmosphere during Raman scattering measurements. Heating or cooling cycles of approximately 80 min duration were performed between 80 K and 700 K. Variable field Hall effect measurements, in combination with quantitative mobility spectrum analysis (QMSA) and multiple-carrier fitting (MCF), were

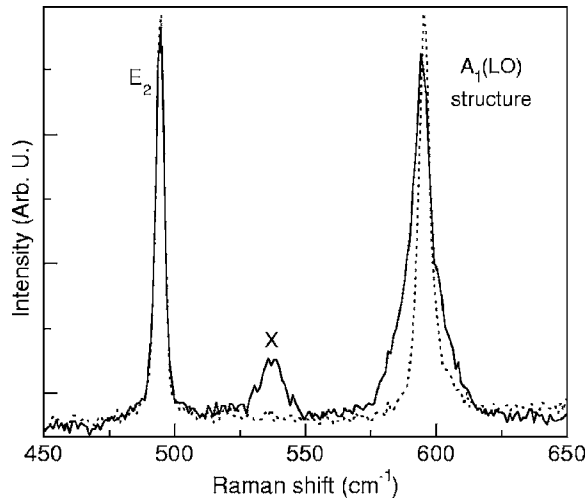


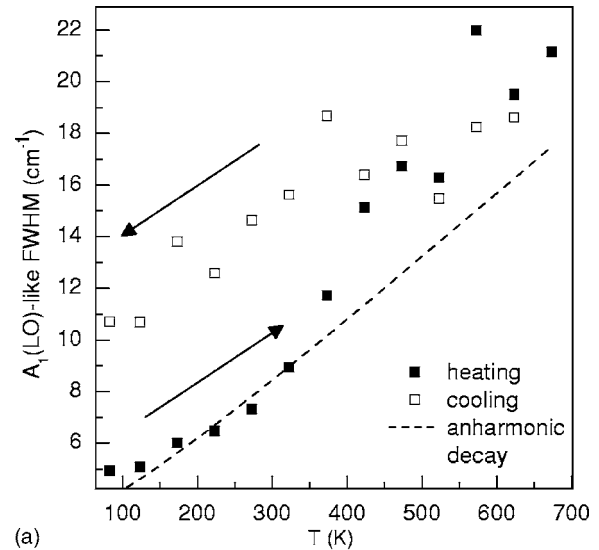
FIG. 1. Raman spectra recorded at 80 K for the as-grown layer (dotted line) and after annealing at 700 K (solid line). An unidentified feature, marked as *X*, is evident at  $\sim 535$   $\text{cm}^{-1}$  in the post-annealed spectrum.

used to extract information about different carriers species present in the layer.<sup>14</sup>

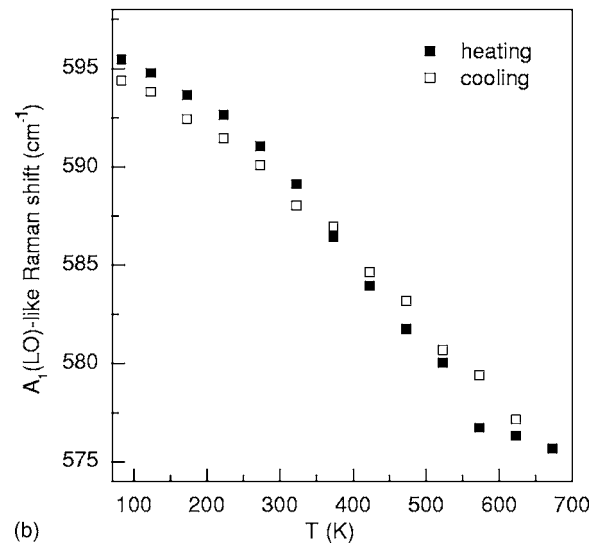
## RESULTS

Figure 1 shows a Raman spectrum of the as-grown InN layer measured at 80 K. The  $E_2$  phonon mode is observed at  $495.5$   $\text{cm}^{-1}$ , higher than the room temperature value of  $490$   $\text{cm}^{-1}$  reported in Ref. 10, consistent with the temperature-dependent frequency shift due to lattice expansion and anharmonic phonon damping. The narrow  $3.8$   $\text{cm}^{-1}$  FWHM spectral width illustrates the high crystalline quality of the InN layer within the depth probed by the laser. The second peak in the Raman spectrum has a spectral width of  $\sim 5$   $\text{cm}^{-1}$  FWHM and is centered at  $595.5$   $\text{cm}^{-1}$ , close to the predicted unscreened  $A_1(\text{LO})$  phonon frequency.<sup>10</sup> No GaN phonon modes originating from the buffer layer are apparent in the Raman spectrum, illustrating that the laser light is absorbed within the InN layer.

The spectral width and frequency of the LO-like phonon, shown in Figs. 2(a) and 2(b), respectively, were determined from Raman spectra recorded during the first annealing cycle using a Lorentzian-Gaussian curve-fitting procedure. The phonon spectral width temperature dependence predicted from anharmonic damping,<sup>6</sup> is shown Fig. 2(a) for reference. The  $A_1(\text{LO})$ -like mode broadens with increasing sample temperature but deviates from the predicted temperature dependence at about 350 K. During cooling, the phonon spectral width decreases, but does not return to the initial as-grown value. Further temperature cycling revealed that the observed LO-like mode broadening is irreversible. We note that after cycling over the whole 80–700 K temperature range, the temperature dependence of phonon broadening is once again consistent with anharmonic damping effects, albeit offset from the original values. The frequency of the LO-like mode shown Fig. 2(b) is redshifted by about  $1$   $\text{cm}^{-1}$  following the annealing cycle, correlating with the irreversible broadening



(a)



(b)

FIG. 2. The phonon spectral width (a) and frequency (b) of the  $A_1(\text{LO})$ -like mode measured during heating and cooling stages of the annealing cycle. The phonon temperature dependence of phonon spectral width predicted by anharmonic damping effects (Ref. 6) is shown as a dashed line in plot (a).

observed for the linewidth. For InN epilayers annealed below 700 K, the  $E_2$  phonon spectral width and frequency measured during heating and cooling cycles are identical within the experimental error. The  $E_2$  phonon spectral width and frequency provide a measure of structural order and strain, respectively. Therefore, no evidence is found for a large structural change occurring within the temperature range investigated. The as-grown and post-annealing Raman spectra measured at 80 K are overlaid in Fig. 1. Comparison between the Raman spectra illustrates that the LO-like mode is visibly broadened and slightly redshifted following annealing, while the  $E_2$  mode remains identical within the experimental error.

A feature apparent at  $535$   $\text{cm}^{-1}$  in the post-annealed spectrum of Fig. 1 is not evident in the as-grown spectrum. This feature has already been reported for as-grown InN layers and was attributed to a  $B_1$  phonon mode,<sup>8</sup> predicted in the

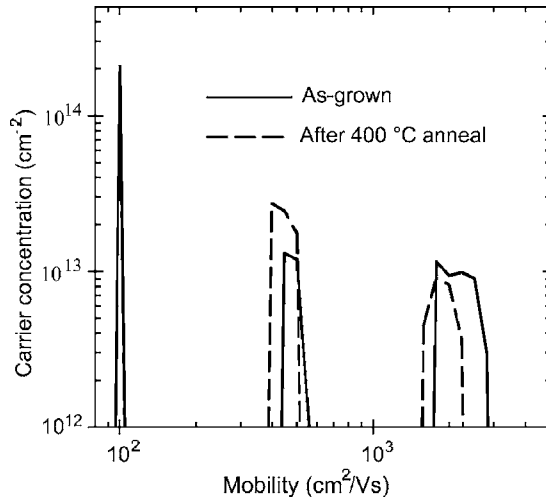


FIG. 3. Mobility spectra (sheet carrier concentration) of the as-grown and annealed InN layer determined from variable field Hall effect measurements at 80 K.

range 530–560  $\text{cm}^{-1}$ ,<sup>10</sup> between the  $E_2$  and  $A_1(\text{LO})$  phonon modes. The  $B_1$  mode is optically inactive and can therefore only contribute to Raman scattering in a disordered lattice due to the breakdown of translational symmetry. Judging by the narrow  $E_2$  phonon spectral width, which is unchanged by annealing the layer, and the fact that no other symmetry forbidden phonon modes are observed, the  $B_1$  mode assignment seems unlikely. The origin of the 535  $\text{cm}^{-1}$  mode is currently unknown to us. However, we note that for InN layers exhibiting annealing-induced LO-like phonon mode broadening, the intensity of this feature increases with temperature when the layer is first heated above 350–400 K.

Figure 3 shows mobility spectra determined from variable field Hall effect measurements of the InN layer at 80 K before and after annealing. At least three different mobility carriers are present. The high mobility carrier, centered at  $\sim 2150 \text{ cm}^2/\text{V s}$ , is associated with the bulk. The low mobility carrier  $< 100 \text{ cm}^2/\text{V s}$  can be associated with a surface conduction layer,<sup>14</sup> while the  $\sim 500 \text{ cm}^2/\text{V s}$  mobility carrier may be related to the InN/buffer interface. Mobility of the  $\sim 500 \text{ cm}^2/\text{V s}$  and  $\sim 2150 \text{ cm}^2/\text{V s}$  carriers decreases after annealing; and there is also a small increase in the concentration of the  $\sim 500 \text{ cm}^2/\text{V s}$  carrier. For the lowest mobility carrier, originating from the surface, only zero mobility conductivity is determined since the mobility is low enough that mobility and carrier concentration cannot be resolved independently.<sup>14</sup> Annealing reduces the conductivity of this carrier by a factor of roughly 1.5.

## DISCUSSION

The irreversible broadening and redshift of the  $A_1(\text{LO})$ -like phonon, illustrated in Figs. 2(a) and 2(b), indicates that permanent changes are induced in the InN layer when it is first heated above 350–400 K. By monitoring the  $E_2$  phonon we can conclude that, in the temperature range investigated, no significant structural changes occur within the  $\sim 60 \text{ nm}$  depth probed by the laser. The mechanism re-

sponsible for the broadening and redshift of the LO-like phonon must therefore be attributed to a change in phonon-plasmon interaction. This is direct evidence that the controversial 595  $\text{cm}^{-1}$  mode is in fact a phonon-plasmon coupled mode and not an unscreened  $A_1(\text{LO})$  phonon. It is therefore justified to assign the 595  $\text{cm}^{-1}$  phononlike mode as a longitudinal phonon-plasmon coupled mode. The behavior illustrated in Fig. 2 was reproduced in several other InN layers,<sup>5</sup> although not all those investigated.<sup>6</sup>

Following the observed annealing induced changes in the  $A_1$ -LPP, it remains centered close to the predicted 590  $\text{cm}^{-1}$   $A_1(\text{LO})$  frequency.<sup>10</sup> To enable comparison to the experimental Raman spectrum, we have calculated the LPP line shape by incorporating the Lindhard-Mermin susceptibility for  $\mathbf{q} \neq 0$  processes. The large wave vector contribution may arise from the presence of impurities in InN,<sup>4,7,8</sup> as well as the laser excitation being resonant with a critical point of InN.<sup>5,9</sup> The method described in the following is similar to that used in Refs. 7 and 12. The total longitudinal dielectric function of a polar lattice can be written as the sum of background (first term), phonon (second term) and free carrier (third term) contributions

$$\varepsilon(q, \omega) = \varepsilon_\infty + \varepsilon_\infty \frac{\omega_{LO}^2 - \omega_{TO}^2}{\omega_{TO}^2 - \omega^2 - i\omega\gamma} + \chi(q, \omega), \quad (1)$$

where  $\varepsilon_\infty$  is the background dielectric constant,  $\omega$  is frequency,  $\mathbf{q}$  is wave vector,  $\gamma$  is the phonon anharmonic damping parameter,  $\omega_{LO}$  and  $\omega_{TO}$  are the longitudinal and transverse phonon frequencies, respectively. The dielectric susceptibility of a free electron gas is given by Lindhard-Mermin expression<sup>15</sup>

$$\chi(q, \omega) = \frac{(1 + i\Gamma/\omega)[\chi^0(q, \omega + i\Gamma)]}{1 + (i\Gamma/\omega)[\chi^0(q, \omega + i\Gamma)/\chi^0(q, 0)]}, \quad (2)$$

where  $\Gamma = \tau^{-1} = e/\mu m^*$  is the electron collision frequency and  $\chi^0(q, \omega + i\Gamma)$  is the temperature-dependent Lindhard expression for the dielectric susceptibility.<sup>16</sup> We use  $T=0 \text{ K}$  to enable the Lindhard expression to be evaluated analytically, a valid assumption for low temperature Raman scattering. The analytical solution of the Lindhard expression is detailed in Ref. 17. We also assume a parabolic conduction band as in Refs. 7 and 12, using  $m^* = 0.09m_e$ . The Raman scattering intensity is determined by integrating all scattering processes up to the cut-off wave vector  $\mathbf{q}_{max}$

$$I(\omega) = \int_0^{q_{max}} q^2 F(q) S(\omega) \text{Im} \left[ -\frac{1}{\varepsilon(q, \omega)} \right] dq, \quad (3)$$

including the Yukawa-type impurity potential weighting function  $F(q)$  for  $\mathbf{q} \neq 0$  processes.<sup>18</sup> The response function  $S(\omega)$  in Eq. (3) is determined by the predominant scattering mechanism and reduces to a constant for the forbidden Fröhlich (IF) scattering mechanism. The integral  $I(\omega)$  converges slowly and is sensitive to  $q_{max}$ , the wave vector limit used. A full review of the application of the Lindhard-Mermin theory to light scattering in semiconductors can be found in Ref. 18.

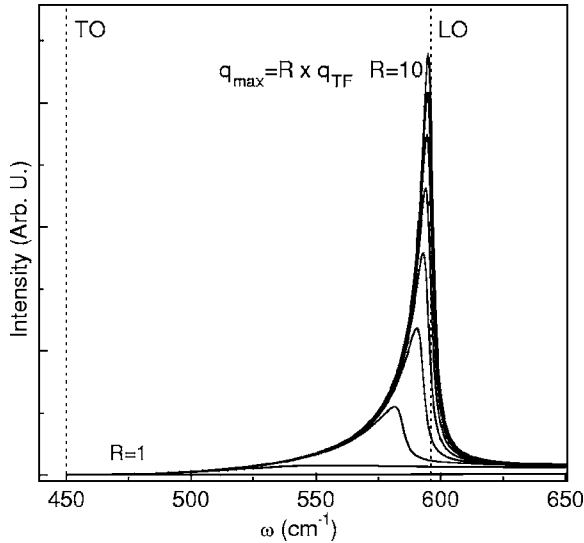


FIG. 4. Longitudinal phonon-plasmon coupled mode line shape calculated using  $\mu=2150 \text{ cm}^2/\text{V s}$ ,  $n=4.5 \times 10^{17} \text{ cm}^{-3}$  for increasing multiples of the Thomas-Fermi screening wave vector ( $q_{TF}$ ). The TO and unscreened  $A_1(\text{LO})$  phonon frequencies are indicated by dashed lines.

The simulated phonon-plasmon coupled mode was calculated by solving Eq. (3) and using the bulk carrier concentration ( $4.5 \times 10^{17} \text{ cm}^{-3}$ ) and mobility ( $2150 \text{ cm}^2 \text{ v}^{-1} \text{ s}^{-1}$ ) parameters determined from the Hall analysis. The values  $\omega_{\text{TO}}=450 \text{ cm}^{-1}$  and  $\omega_{\text{LO}}=596 \text{ cm}^{-1}$  used here are similar to those reported in Ref. 10. Increasing  $q_{\text{max}}$  causes the  $L^-$  LPP branch to blue-shift, plotted in Fig. 4 for increasing multiples of the Thomas-Fermi screening wave vector ( $q_{TF}$ ). The  $L^-$  mode converges to the unscreened LO phonon frequency for large wave vectors, in agreement with Refs. 6 and 7. The  $L^+$  branch shifts to higher energy and is ultimately Landau damped and ceases to exist for large wave vectors<sup>18</sup> (not shown). We note that for small  $q$  values, the calculated LPP line shape exhibits  $L^-$  and  $L^+$  branches below the TO phonon frequency and above the LO frequency, respectively. The IIF scattering mechanism response function  $S_{\text{IIF}}(\omega)$  has been used in Eq. (3) and gives the best agreement possible with the experimental peak shape. The IIF mechanism is dominant for excitation energies near to critical point resonances, illustrated in Ref. 12 for excitation close to the fundamental band gap of GaN. The assignment of IIF scattering in the current work is consistent with the above-band gap resonance-enhanced LO-phonon scattering previously observed for InN,<sup>5</sup> although we make no assumptions about the exact nature of the critical point or its relation to the band gap. The response function for the charge density fluctuation (CDF) scattering mechanism,  $S_{\text{CDF}}(\omega)$ , has a maximum at  $\omega_{\text{TO}}$  and minimum at  $\omega_{\text{LO}}$ ,<sup>18</sup> and therefore does not reproduce the experimental line shape well (not shown). In Fig. 5, the simulated LPP is overlaid with the experimental spectrum for comparison. The simulated LPP mode frequency agrees well with the experimental  $A_1(\text{LO})$ -like mode, although it exhibits an asymmetry not observed in the experimental spectrum. Since this material is electrically inhomogeneous, it is likely that the LO-like mode is in fact

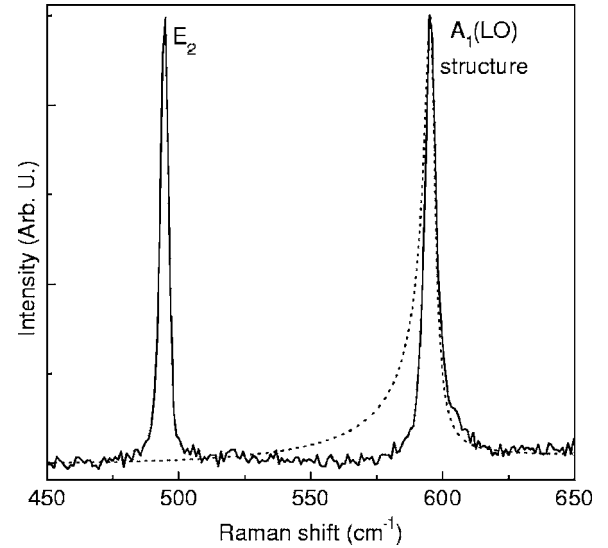


FIG. 5. As-grown Raman spectra recorded at 80 K (solid line) overlaid with phonon-plasmon coupled mode (dotted line) simulated for  $q_{\text{max}}=15q_{TF}$ ,  $\mu=2150 \text{ cm}^2/\text{V s}$ , and  $n=4.5 \times 10^{17} \text{ cm}^{-3}$ .

superposition of LPP modes arising from more than one conduction layer. This may make the exact fitting of the simulated LLP line shape to the experimental spectrum difficult.

To investigate whether the annealing induced changes in the carrier mobility could account for the observed broadening of the LO-like mode shown in Fig. 2(a), the LPP line shape was calculated for a range of carrier mobilities. Considering the bulk carrier concentration determined from the Hall measurements ( $4.5 \times 10^{17} \text{ cm}^{-3}$ ), and using mobilities encompassing both medium and high mobility carriers ( $250\text{--}2200 \text{ cm}^2/\text{V s}$ ), the calculated line shape does not vary significantly from the one overlaid in Fig. 5. Only when the mobility is reduced further,  $<250 \text{ cm}^2/\text{V s}$ , does the calculated  $L^-$  LPP broaden significantly with decreasing mobility, shown in Fig. 6. The measured trend of decreasing carrier mobility after annealing is therefore consistent with the LPP broadening. However, the mobility decrease measured for medium and high mobility carriers is not large enough to account for the experimental observed broadening. Adjusting the carrier concentration in the range measured for high and medium mobility carriers ( $0.4\text{--}1.2 \times 10^{18} \text{ cm}^{-3}$ ) also did not significantly change the calculated LPP line shape (not shown).

Figure 6 does illustrate that low mobility carriers may be responsible for the observed annealing induced broadening of the LPP. The conductivity of the low mobility surface related carriers shows a reduction by a factor of 1.5 post annealing. Unfortunately, the exact carrier concentration and mobility are difficult to resolve in the surface conduction layer using the variable field Hall method. Exact parameters required for fitting the LPP are therefore not available. Using a very low carrier mobility,  $\mu=25 \text{ cm}^2/\text{V s}$  for example, the LPP line shape calculated for carrier concentrations of  $1 \times 10^{17} \text{ cm}^{-3}$  and  $1 \times 10^{18} \text{ cm}^{-3}$  is shown in Fig. 7. The resulting spectral width is  $\sim 9 \text{ cm}^{-1}$  FWHM and a small redshift is observed for the higher carrier concentration, similar to the experimental spectrum. Therefore, we may speculate

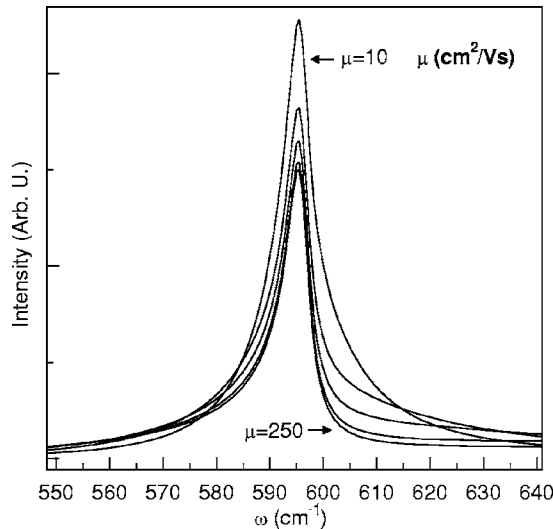


FIG. 6. Simulated phonon-plasmon coupled mode line shapes for  $q_{max}=15q_{TF}$  and  $n=4.5 \times 10^{17} \text{ cm}^{-3}$  with electron mobilities: 250 (inner curve), 125, 50, 25, and 10 (outer curve)  $\text{cm}^2/\text{V s}$ .

that the low mobility carriers ( $<100 \text{ cm}^2/\text{V s}$ ), associated with the surface, are involved in the experimentally observed broadening of the LO-like mode post annealing (from 5 to  $10 \text{ cm}^{-1}$  FWHM). Considering the low thermal stability of InN,<sup>19</sup> it is possible that nitrogen decomposition at the surface generates a small concentration of nitrogen vacancies. This would reduce mobility, but may not be apparent in the  $E_2$  linewidth which typically requires larger structural changes. In this case, we may also speculate that the currently unexplained feature at  $535 \text{ cm}^{-1}$  is related to nitrogen decomposition near the sample surface.

### CONCLUSIONS

To gain insight into the interaction between carriers and polar phonons in InN, Raman spectra were recorded during annealing cycles between 80–700 K. The observed irreversible broadening and redshift of the  $A_1(\text{LO})$ -like phonon mode indicates that a permanent change is induced in when the InN layer is first heated above 350–400 K. Since no effect was observed for the nonpolar  $E_2$  phonon, this is direct evidence of LO phonon-plasmon interaction in InN. Variable

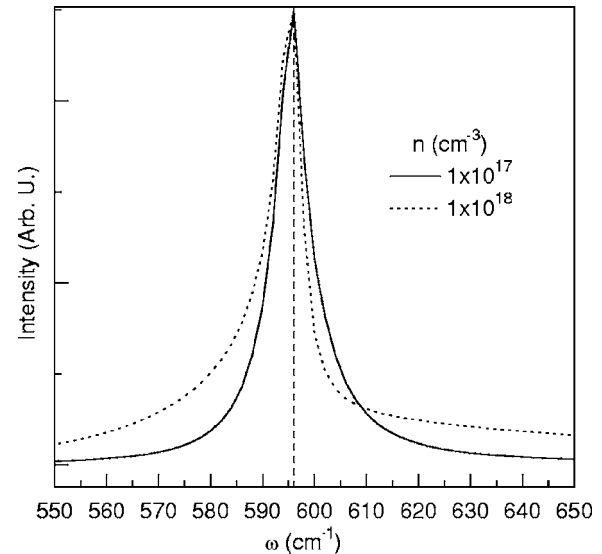


FIG. 7. Simulated phonon-plasmon coupled mode line shapes for  $q_{max}=15q_{TF}$ ,  $25 \text{ cm}^2/\text{V s}$  mobility and carrier concentrations of  $1 \times 10^{17} \text{ cm}^{-3}$  and  $1 \times 10^{18} \text{ cm}^{-3}$ . The  $A_1(\text{LO})$  frequency is indicated by a dashed line.

field Hall effect measurements revealed that the InN layer is electrically heterogeneous, with at least three conduction layers associated with the bulk, surface, and interface. Measured carrier mobility decreases after annealing. The simulated  $L^-$  phonon-plasmon coupled mode converges close to the unscreened  $A_1(\text{LO})$  frequency for large wave vectors. However, while the spectral width of the simulated phonon-plasmon line shape increases with decreasing electron mobility, consistent with the Raman data, the changes observed for the high and medium mobility carriers are not large enough to account for the experimentally observed broadening of the LO-like mode after annealing. We speculate that the surface is modified by annealing the sample to 700 K, affecting surface conduction carriers and resulting in the observed broadening of the  $A_1(\text{LO})$ -like mode.

### ACKNOWLEDGMENTS

We thank T. Suski (Unipress) for complimentary Hall measurements of the samples investigated here and discussion. We also thank A. Sarua (University of Bristol) for helpful discussion.

<sup>1</sup>A. G. Bhuiyan, A. Hashimoto, and A. Yamamoto, J. Appl. Phys. **94**, 2779 (2003).

<sup>2</sup>H. Lu, W. J. Schaff, J. Hwang, W. Wu, G. Koley, and L. F. Eastman, Appl. Phys. Lett. **79**, 1489 (2001).

<sup>3</sup>V. Y. Davydov, A. A. Klochikhin, M. B. Smirnov, V. V. Emtsev, V. D. Petrikov, I. A. Abroyan, A. I. Titov, I. N. Goncharuk, A. N. Smirnov, V. V. Mamutin, S. V. Ivanov, and T. Inushima, Phys. Status Solidi B **216**, 779 (1999).

<sup>4</sup>A. Kasic, M. Schubert, Y. Saito, Y. Nanishi, and G. Wagner, Phys. Rev. B **65**, 115206 (2002).

<sup>5</sup>M. Kuball, J. W. Pomeroy, M. Wintrebort-Fouquet, K. S. A. Butcher, H. Lu, W. J. Schaff, T. V. Shubina, S. V. Ivanov, A. Vasson, and J. Leymarie, Phys. Status Solidi A **202**, 763 (2005).

<sup>6</sup>J. W. Pomeroy, M. Kuball, H. Lu, W. J. Schaff, X. Wang, and A. Yoshikawa, Appl. Phys. Lett. **86**, 223501 (2005).

<sup>7</sup>F. Demangeot, C. Pinquier, J. Frandon, M. Gaio, O. Briot, B. Maleyre, S. Ruffenach, and B. Gil, Phys. Rev. B **71**, 104305 (2005).

<sup>8</sup>J. S. Thakur, D. Haddad, V. M. Naik, R. Naik, G. W. Auner, H. Lu, and W. J. Schaff, Phys. Rev. B **71**, 115203 (2005).

- <sup>9</sup>J. W. Ager III, W. Walukiewicz, W. Shan, K. M. Yu, S. X. Li, E. E. Haller, H. Lu, and W. J. Schaff, *Phys. Rev. B* **72**, 155204 (2005).
- <sup>10</sup>G. Kaczmarczyk, A. Kaschner, S. Reich, A. Hoffmann, C. Thomsen, D. J. As, A. P. Lima, D. Schikora, K. Lischka, R. Averbeck, and H. Riechert, *Appl. Phys. Lett.* **76**, 2122 (2000).
- <sup>11</sup>D. Olego and M. Cardona, *Phys. Rev. B* **24**, 7217 (1981).
- <sup>12</sup>M. Ramsteiner, O. Brandt, and K. H. Ploog, *Phys. Rev. B* **58**, 1118 (1998).
- <sup>13</sup>A. Kasic, E. Valcheva, B. Monemar, H. Lu, and W. J. Schaff, *Phys. Rev. B* **70**, 115217 (2004).
- <sup>14</sup>C. H. Swartz, R. P. Tompkins, N. C. Giles, T. H. Myers, H. Lu, W. J. Schaff, and L. F. Eastman, *J. Cryst. Growth* **269**, 29 (2004).
- <sup>15</sup>N. D. Mermin, *Phys. Rev. B* **1**, 2362 (1970).
- <sup>16</sup>J. Lindhard, *K. Dan. Vidensk. Selsk. Mat. Fys. Medd.* **28**, 881 (1954).
- <sup>17</sup>S. Ernst, A. R. Goni, K. Syassen, and M. Cardona, *Phys. Rev. B* **53**, 1287 (1996).
- <sup>18</sup>G. Abstreiter, M. Cardona, and A. Pinczuk, in *Light Scattering in Solids*, edited by M. Cardona (Springer, Berlin, 1984), Vol. IV, p. 5.
- <sup>19</sup>O. Ambacher, M. S. Brandt, R. Dimitrov, T. Metzger, M. Stutzmann, R. A. Fischer, A. Miehr, A. Bergmaier, and G. Dollinger, *J. Vac. Sci. Technol. B* **14**(6), 3532 (1996).